Predictability and Spectral Truncation

FERDINAND BAER

Dept. of Atmospheric and Oceanic Science, The University of Michigan, Ann Arbor 48104

FRED N. ALYEA

Dept. of Meteorology, Massachusetts Institute of Technology, Cambridge 02108

(Manuscript received 17 August 1973, in revised form 31 January 1974)

ABSTRACT

A quasi-geostrophic, two-level baroclinic model with a fixed heating function and simple friction represented in spectral form was integrated with climatological initial conditions for 30 days. Three separate integrations were performed changing only the spectral truncation. Two of the experiments had 10 degrees of freedom in latitude with 16 and 20 planetary waves, while the third had 11 degrees of latitudinal freedom and 18 planetary waves. Comparison of the integration results indicates that the increase in latitudinal resolution caused pronounced changes in the predicted variables whereas the increase in the number of planetary waves had a negligible effect on the distribution of variables over the integration period.

1. Introduction

Although the ultimate predictability of atmospheric flow may be absolutely limited (Lorenz, 1969), both the approach to this limit and the accuracy of forecast during this approach are strongly related to truncation. By truncation we here refer to the conversion of the appropriate set of differential equations describing the flow to computational form (either finite-difference or spectral) and the number of degrees of freedom ultimately chosen to represent the flow development in time. It is, of course, evident that because we are dealing with a highly nonlinear system, each additional degree of freedom (grid point or spectral expansion coefficient) will allow for additional scale interaction thus providing improved predictability. Experiments have indeed verified this expectation as may be noted from the studies of Miyakoda *et al.* (1971), Wellck *et al.* (1971) and Baer and Alyea (1971). The first two studies were performed by finite-difference methods, the latter by a spectral expansion.

The spectral expansion method when utilized for truncation studies has a distinct advantage. The addition of degrees of freedom from one experiment (truncation) to another can be performed with great simplicity and independently of the number of degrees of freedom chosen. This is to be contrasted with the grid-point method, wherein any modification other than doubling or halving the grid becomes a burdensome operation. One may further note that the dependence of computational accuracy on scale becomes immediately apparent in the spectral domain. We have consequently chosen the spectral method to perform the truncation experiments to be discussed in this sequel to the earlier study (Baer and Alyea, 1971).

The previous studies referred to above did suggest that the addition of predictable scales to a forecast model (more degrees of freedom) resulted in superior forecasts. They did not indicate if any limits existed in this process; i.e., if continued addition of degrees of freedom might ultimately be of no additional forecast benefit. Nor did they indicate whether the addition of degrees of freedom in special ways might be consequential to the forecast. It is to this latter question that we should like to address the reader's attention.

In the previous study by the writers (Baer and Alyea, 1971; subsequently to be referred to by the acronym SPTI) there was some indication that for a given accuracy in latitude, the addition of planetary waves beyond a certain number did not yield altered predictions over the integration period, which, in that case, was 30 days. The implication of this result was either that an optimum truncation had been established or that the predictability was somehow related strongly to latitudinal resolution. The latter conclusion has been borne out by the experiments to be described herein.

We have integrated the model used in SPTI with climatological initial conditions (as contrasted to spin-up conditions used previously) and with a somewhat modified forcing function. The climatological initial conditions present a zonal field with small-amplitude waves such that the prediction model will show the details of wave development. Three spectral truncations were tested and integrations were performed for 30 days. Significant parameters of the flow, principally

energy in wave components, were observed as they developed during the integrations and were compared among the three experiments. In this way we were able to detect if and when truncation influenced the forecast. We shall again attempt to avoid assessing the forecasts in terms of "reality" since we do not wish to evaluate the model, but rather focus attention on the results as they relate one prediction (truncation experiment) to another. An additional note of interest was a comparative test between the interaction coefficient integration scheme and the Gaussian quadrature scheme (Machenhauer and Rasmussen, 1972) for comparable truncation. At the truncation levels used for this study, no benefit accrued to the quadrature scheme.

2. Model and representation

The model used to perform the integrations for various truncations is identical to the one used in SPTI and will not be repeated in detail here. It is a simple baroclinic model based on the energetically consistent systems developed by Lorenz (1960) and used initially for general circulation studies by Phillips (1956). The purpose of utilizing such a simple system is to avoid complexities in the physics as well as reducing computational requirements, yet maintaining a semblance of reality.

Listed under its assumptions, the model is quasi-geostrophic, quasi-hydrostatic, has fixed static stability, includes horizontal diffusion, vertical shearing stresses both internally and at the lower boundary, and has a forcing function which is represented by a latitudinally dependent heating function. Represented in pressure coordinates in a two-level form, the dependent variables are evaluated at surfaces corresponding to 250 and 750 mb, with the individual pressure derivative (ω) specified to vanish both on the top ($p=0$) and the bottom ($p=1000$ mb) boundaries. By virtue of the geostrophy of the model, the horizontal wind field is represented by its rotational component (streamfunction) through the conventional definition, $\mathbf{V}=\mathbf{k}\times\nabla\psi$, where $\mathbf{k}$ is a unit vector normal to the spherical pressure surface. Because of the two levels of information, one may generate four dependent variables; both streamfunctions and temperatures at 750 and 250 mb. Following Lorenz (1960), these variables may be converted to a mean stream field (ψ), a shear stream field (τ), a mean potential temperature (θ), and a temperature shear or stability parameter (σ). We have already noted that σ is chosen constant. Furthermore, the mean temperature can be directly related to the stream shear through the thermal wind. Thus the final differential system has only the two dependent variables (ψ,τ) which must be predicted. The ultimate prediction equations are given as [see also Eqs. (10), SPTI]:

$$\left.\begin{aligned}&\frac{\partial}{\partial t}\nabla^2\psi+L_1\psi-2C_2'\nabla^2\tau=-J(\psi,\nabla^2\psi)-J(\tau,\nabla^2\tau)\\&\frac{\partial}{\partial t}(\nabla^2\tau-a^2\delta^2\tau)+L_2\tau-C_2'\nabla^2\psi=\\&\qquad-J(\psi,\nabla^2\tau-a^2\delta^2\tau)-J(\tau,\nabla^2\psi)-\frac{f_0H}{\sigma\Omega}\end{aligned}\right\}. \quad (1)$$

The operators L in (1) are linear and include the effects of dissipation as well as the advection of the earth's vorticity. Diffusive effects are incorporated in the constants C and stability is involved in δ. The variables, both dependent and independent, have been nondimensionalized in space by the earth's mean radius (a) and in time by its rotation rate (Ω). Complete details of the development of (1) may be found in SPTI.

For integration purposes, (1) were converted to spectral form by substituting the expansion

$$\begin{pmatrix}\psi\\ \tau\end{pmatrix}=\sum_\gamma\begin{pmatrix}\psi_\gamma\\ \tau_\gamma\end{pmatrix}Y_\gamma(\lambda,\mu)=\sum_\gamma\zeta_\gamma Y_\gamma, \quad (2)$$

thus reducing the partial differential equations to a set of nonlinear ordinary differential equation in time alone. The expansion coefficients (ζ_γ) are time-dependent and must be predicted for all chosen wave vectors $\gamma=n_\gamma+il_\gamma$, which include the rank and degree of the solid harmonics $Y_\gamma(\lambda,\mu)$ where λ represents longitude and μ is the sine of latitude. The properties of the solid harmonics, Fourier series in longitude and Legendre polynomials in latitude, and their applicability to meteorological problems may be found in Platzman (1960). The procedure for generating the spectral equations is also described in SPTI and yields the prediction equation

$$\frac{d\zeta_\gamma}{dt}-\mathbf{B}_\gamma\zeta_\gamma=\mathbf{R}_\gamma. \quad (3)$$

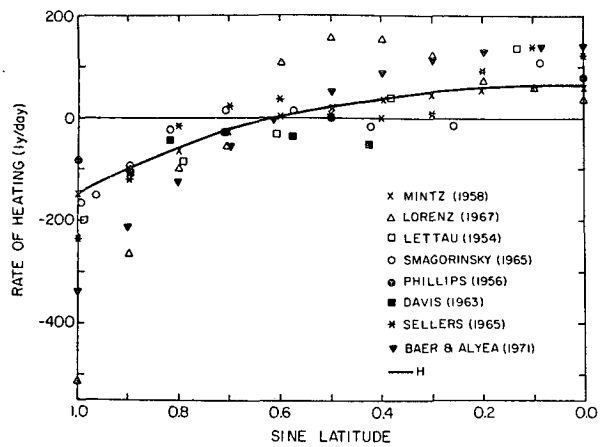

FIG. 1. Heating rates (ly day^{-1}) as a function of latitude from observations and for various numerical models.

All linear effects have been incorporated into the matrix $\mathbf{B}_\gamma$ so that $\mathbf{R}_\gamma$ includes only nonlinear scale interaction and the heating (forcing) function, which is inhomogeneous for our problem.

For the time integration of (3), we have chosen the leap-frog scheme with periodic restart, but treat the linear terms exactly (without time truncation) since reduction in truncation errors is thereby achieved (see, for example, Baer and Simons, 1970). The final prediction system is then given as

$$\zeta_\gamma^{t+\Delta t}=\exp(2\mathbf{B}_\gamma\Delta t)\zeta_\gamma^{t-\Delta t}+2\Delta t\exp(\mathbf{B}_\gamma\Delta t)\mathbf{R}_\gamma^t. \quad (4)$$

If only the initial ζ_γ is specified for all γ, and the heating function is described, the integration may proceed. The basic question to be considered in this study involves the development of (ψ) as it depends on the number of wave vectors (γ) chosen. We shall specify these truncations in the following section.

3. Forcing, truncation and initialization

The heating function utilized in (1) and denoted by H is essentially the same in form as the one used in SPTI. It is purely inhomogeneous, dependent only on latitude and is thus similar to that used by Phillips (1956). However, we noted that our previous function was somewhat too strong and we have thus reduced its amplitude while maintaining its shape. Fig. 1 describes the heating functions used both by modelers (Phillips, 1956; Mintz, 1958; Smagorinski *et al.*, 1965; Baer and Alyea, 1971), as well as estimates taken from observations (Davis, 1963; Lettau, 1954; Sellers, 1965; Lorenz, 1967). Although a wide range of values exist, as attested to by the figure, heating at the equator and cooling at the pole are common attributes.

Our heating function may be represented as a series expansion in zonal harmonics (zero planetary wave) with only two even polynomials. As the term enters (1), however, the function becomes odd and is represented by the three lowest odd zonal components with wavenumbers $\gamma=1, 3, 5$. Thus, only those three components of the flow will be directly forced. The details of this development may be found in SPTI with reduced values of the heating coefficients, as seen from Fig. 1.

No specification has yet been made about the terminus of the series (2) which represents the set of dependent variables to be predicted. Indeed the specification of this terminus defines the truncation for the ensuing integration. Basically, we set the truncation point by defining a maximum wave vector $\gamma_N=\gamma_{\max}$ such that the entire set of γ includes N vectors. There are, however, many ways to make the choice, and we must define a systematic procedure to generate truncation experiments. Traditionally, planetary waves have been a focal point in atmospheric flow considerations. In keeping with this tradition, we first choose a truncation point on the planetary wave index l_γ; thus, we choose $l_{\max}$ and include all planetary waves in the range of wavenumbers $0\leqslant l_\gamma\leqslant l_{\max}$. We may now select the resolution in latitude for each of the planetary waves (l_γ). Noting the constraints that $n_\gamma\geqslant l_\gamma$ and that we wish only odd functions, $n_\gamma+l_\gamma=$odd integers, we choose an index m such that each planetary wave has the same number of degrees of freedom in latitude. Our truncation limit N is now set by the range

$$\left.\begin{aligned} &0\leqslant l_\gamma\leqslant l_{\max} \\ &n_\gamma=l_\gamma+2j-1, \quad 1\leqslant j\leqslant m \end{aligned}\right\}, \quad (9)$$

leaving us with a set of wave vectors $N=m(2l_{\max}+1)$. This truncation scheme is denoted as rhomboidal and has been shown by Ellsaesser (1966) to yield satisfactory results on integration. The index n may be recognized as the order of the Legendre polynomial and may also be considered a two-dimensional wavenumber in a spherical surface (see Baer, 1972). [A graphical representation of this form of truncation set may be found in Fig. 2 of SPTI.] A truncation experiment may be simply identified by combining the two integers which define it, $l_{\max}$ followed by m, so that an example of an experiment identifier would be 1610, implying 16 planetary waves $(l_{\max})$ and 10 latitudinal degrees of freedom (m).

In our previous investigations the maximum truncation experiment was 1610. We noted at that time some close similarity between the experiments 1410 and 1610 over an integration period up to 30 days while no other truncations showed such similarity. Because of changes in the heating function and also the initial conditions, we have chosen to repeat the 1610 experiment and add experiments 2010 and 1811. If 10 degrees of latitudinal resolution is sufficient to predict the behavior of the longer planetary waves independently of the number of shorter waves, then the new experiments will indicate the sensitivity of truncation to latitudinal resolution. Details of these experiments may be found in Table 1. The table includes the number of vectors in each experiment, the integration period, time increment, and number of interaction coefficients. The interaction coefficients represent the number of elements forming nonlinear products in the matrix $\mathbf{R}_\gamma$ and is closely related to the computing time necessary for the experiment. Note that experiments 2010 and 1811 have nearly the same number of interactions while experiment 1610 has substantially less. Subsequent analysis will show that the number of interactions is *not* the

TABLE 1. Pertinent data describing truncation properties of various experiments for which integrations were performed.

Identifier	$l_{\max}$	$n_{\max}$	m	Number of vectors	Period (days)	Δt (hr)	Number of interaction coefficients
1610	16	35	10	330	30	0.25	152, 726
2010	20	39	10	410	30	0.25	240, 546
1811	18	39	11	407	30	0.25	255, 854

critical factor in determining prediction characteristics of an experiment.

In terms of corresponding grid-point resolution, the minimum grid interval determined from transformation formulas corresponds to two grid points per wave. Thus, 20 planetary waves could correspond to a mesh length of 1000 km at the equator. However, because of truncation, this limit cannot be reached; indeed, Grammeltvedt (1969) suggests, from observational studies, that in excess of 15 grid points are necessary to describe a wavelength for prediction purposes. We are thus left with a rather loose interpretation of equivalence between wavelength and grid truncation. Certain computational errors in prediction are significantly reduced in the spectral domain, giving added advantage to the technique for the purpose at hand.

Having now established the truncation experiments, we may specify the initial values of the expansion coefficient vectors ζ_γ, thereby completing all conditions necessary to perform the integrations. In our previous experiments (SPTI) we specified the initial state by beginning with no motion and allowing the forcing to establish a zonal field to which wave motion was unstable. Because of the nature of the forcing, this zonal field (see Fig. 2) was somewhat unrealistic when compared to atmospheric observations. Consequently, we have chosen climatological statistics as initial conditions for the present experiments. Normal April climatology was used, and the zonal wind field is depicted in Fig. 2 taken from the data of Crutcher and Meserve (1970) and made available from NCAR. Note that the observed jet is considerably south of the jet as determined by forcing alone, and that the amplitude is also

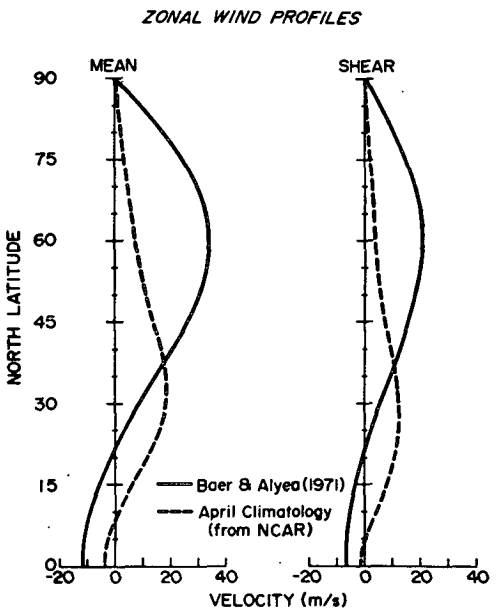

FIG. 2. Initial zonal wind profiles of both the mean and shear flow for the present experiments as well as previous experiments (Baer and Alyea, 1971).

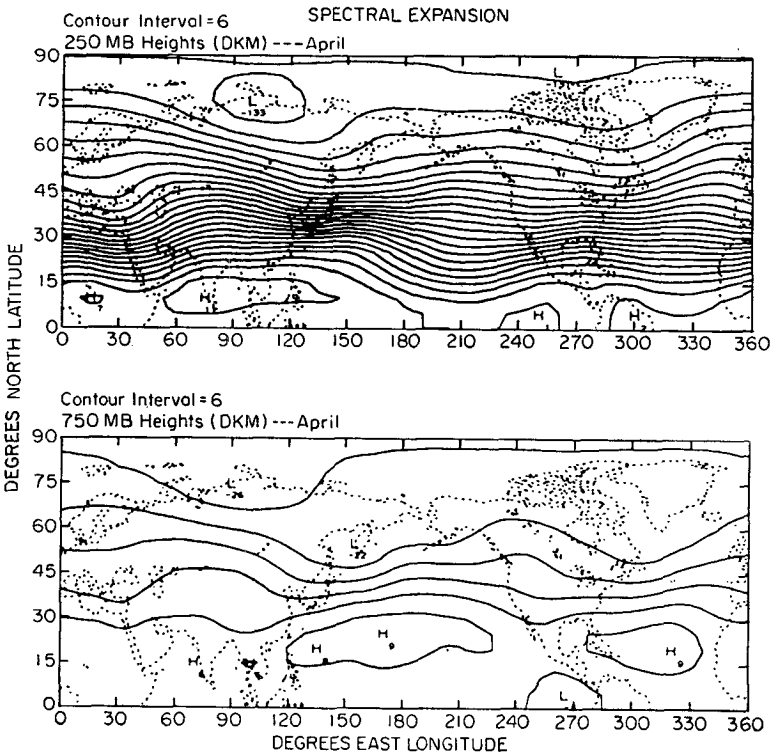

FIG. 3. Initial height field over the Northern Hemisphere at 250- and 570-mb levels taken from April climatology and utilized in the integrations.

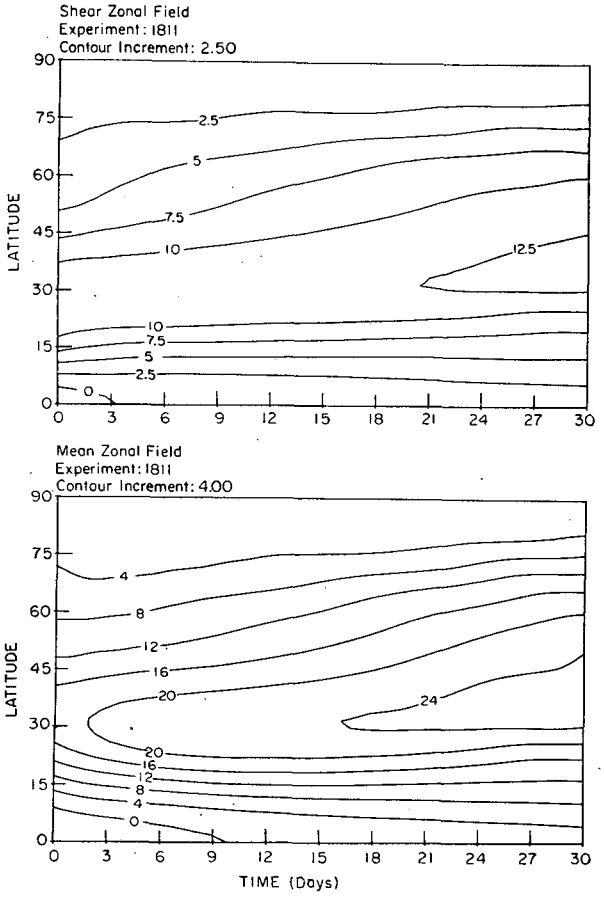

FIG. 4. Time development of zonal wind field (m sec^{-1}) with latitude for both the mean and shear zonal flow fields.

significantly less. The height field, which includes wave data, is shown in Fig. 3 for both the 250- and 750-mb surfaces. In terms of spectral coefficients, the data were analyzed for 16 planetary waves with 8 degrees of latitudinal freedom. We see, as anticipated, that wave activity in the climatological data is rather weak; we will thus be able to observe wave development as a function of truncation and time from low energy levels.

4. Data analysis

To depict the development of our experiments in time, we have chosen to concentrate attention primarily on the energy in the zonal field and the waves, both kinetic energy and available potential energy. Although we shall ignore the development of phase, it is evident from the nonlinearity of our prediction system that substantial errors in phase will be reflected in amplitude errors. For a discussion of the interaction of phase and amplitude errors, see Baer and Simons (1970).

The energy in the wave components (γ) are given by the definitions:

$$\left.\begin{aligned} \bar{K}_\gamma &\equiv c_\gamma \psi_\gamma \psi_\gamma^*, \quad & K_\gamma' &= c_\gamma \tau_\gamma \tau_\gamma^* \\ A_\gamma &\equiv a^2\delta^2 \tau_\gamma \tau_\gamma^*, \quad & K_\gamma &\equiv \bar{K}_\gamma + K_\gamma' \end{aligned}\right\}, \tag{6}$$

where $\bar{K}_\gamma$ is the mean kinetic energy in the component γ, K_γ' the shear kinetic energy, K_γ the total kinetic energy, and A_γ the available potential energy. In (6) the coefficients c_γ represent the eigenvalues of the Legendre polynomials satisfying Laplace's equation in a spherical surface and may be considered as two dimensional scale indices related to the order of the polynomials: $c_\gamma \equiv n_\gamma(n_\gamma+1)$. The total energy in each category (energy over the entire domain) is clearly seen to be the sum of the individual wave energies as defined by (6) over all allowed γ (i.e., over the entire range of truncation as defined in Section 3), and the total energy in the entire system would simply be the sum of the two kinetic energies and the available potential energy. We shall define these energies identically to the energies in the individual scale but without the γ subscript.

It is also convenient to consider the energy in a given planetary wave (l), i.e.,

$$\left.\begin{aligned} K_l &\equiv \sum_{n_\gamma} K_\gamma(l) \\ A_l &\equiv \sum_{n_\gamma} A_\gamma(l) \end{aligned}\right\}, \tag{7}$$

so that the energy in the zonal flow would be given for $l=0$ and the eddy energy would be the sum of all K_γ or A_γ for $l\neq 0$. In a similar vein, the energy in any two-dimensional scale (n) as contrasted to the one-dimensional scale (l)—see Baer (1972)—may be calculated by summing over all l for given n:

$$\left.\begin{aligned} K_n &\equiv \sum_{l_\gamma} K_\gamma(n) \\ A_n &\equiv \sum_{l_\gamma} A_\gamma(n) \end{aligned}\right\}. \tag{8}$$

The effect of truncation may be elucidated by displaying the time development of energy for each experiment and for the differences in energy for any given component from two experiments. We shall see from these displays the relationship among the experiments and how their integrations deviate with time. We shall, finally, display the development of the shorter scales in each experiment with time. We shall do this by fitting those scales statistically to a power law relationship. Such a power law relationship has been anticipated from the theory of two-dimensional and three-dimensional turbulence (e.g., Kraichnan, 1967; Charney, 1971) and one may hope to find a -3 power distribution in the appropriate scale range.

5. Zonal flow

The time development of the zonal velocity, whose initial distribution is given in Fig. 2, may be described graphically on a time section with latitude on the ordinate and time on the abcissa. Such a diagram with isopleths drawn in units of meters per second is presented in Fig. 4 for experiment 1811 for both the mean

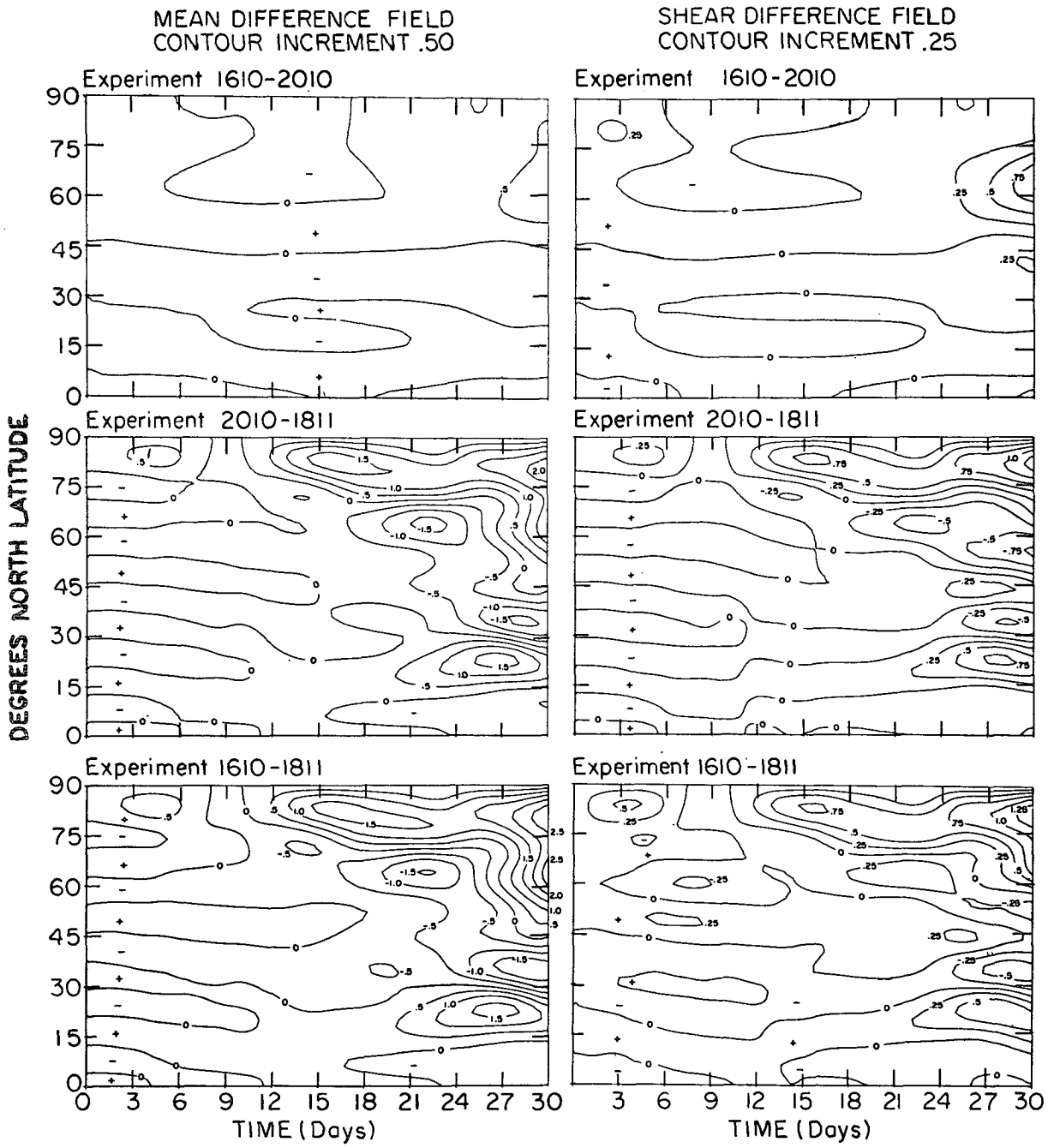

FIG. 5. Time developments of the difference (m sec^{-1}) in zonal mean and shear wind between any two experiments for all permutations of the three experiments.

and shear zonal flow field. No dramatic changes are notable; the jet moves slightly to the north and intensifies by perhaps 20–25% over the period of 30 days, properties common to both the mean and the shear fields. The corresponding development for experiments 1610 and 2010 are quite similar and need not be displayed.

More interesting, however, is the difference in the zonal field development from one experiment to another. These difference fields are described in Fig. 5 by analyzing the difference in zonal flow between two experiments on graphs similar to Fig. 4. Most striking is the insignificant difference in mean zonal flow development between experiments 1610 and 2010, with a comparable behavior in the shear difference field. In contrast, the difference field between experiments 2010 or 1610 and 1811 show substantial variation, beginning at about 15 days into the integration. The deviations in the flow

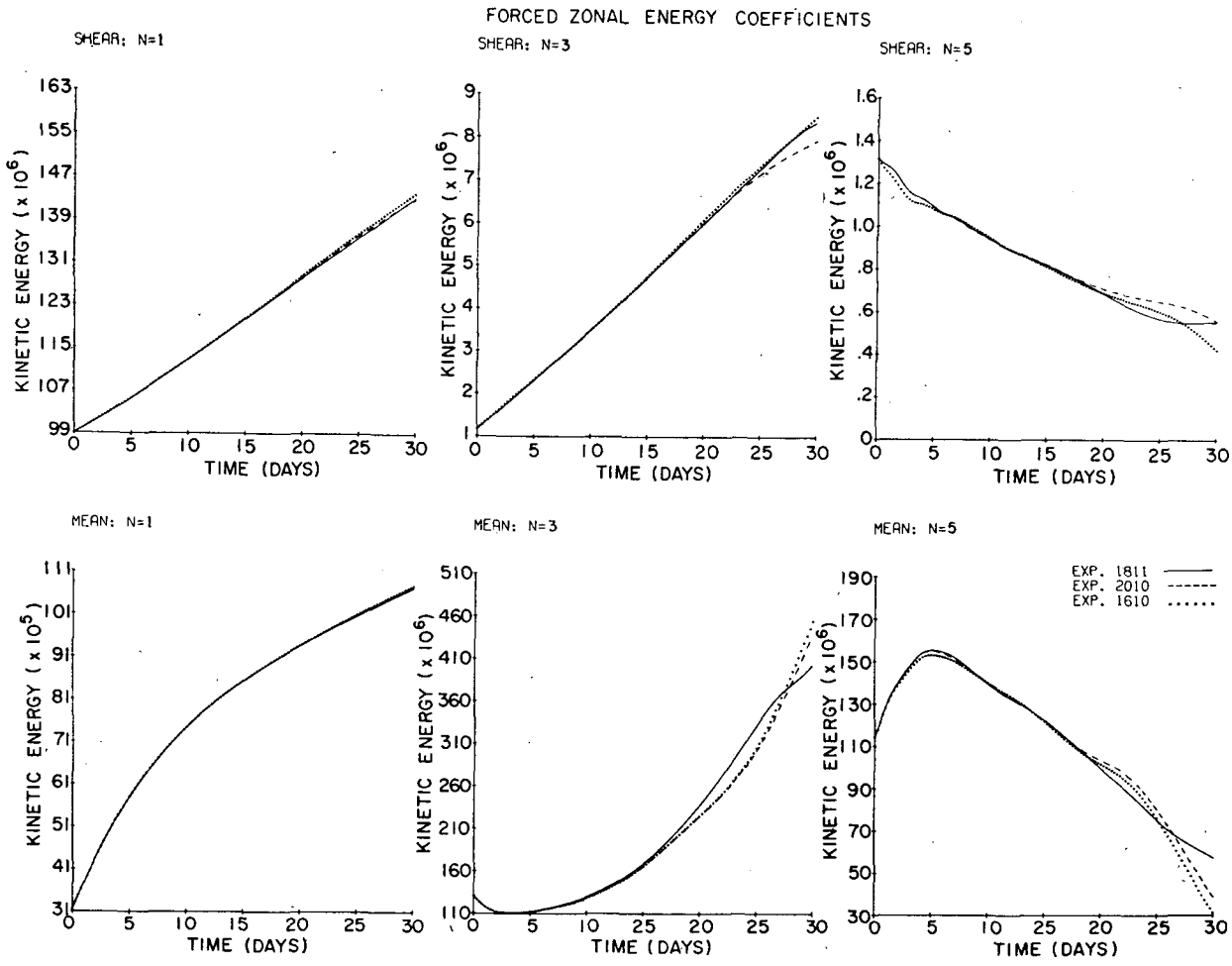

FIG. 6. Time development of energy in the first three (forced) zonal wave components denoted as $\gamma=n=1, 3, 5$ for both the shear and mean in nondimensional units and for all three experiments.

field begin in the north and move south gradually in time to ultimately cover almost the entire latitudinal belt. We are thus led to our first indication that experiment 1811 deviates substantially from the other two experiments in its temporal development (at least in the zonal flow) and experiments 1610 and 2010 follow one another rather closely in their integrations.

Since the zonal flow consists of a series of "wave" components $(\psi_\gamma, \tau_\gamma)$, the time development of these may be followed. Of particular interest are the first three components $(\gamma=1, 3, 5)$ since these components are forced by the heating function. We describe this development of the energy coefficients of both the mean and the shear field in Fig. 6. Despite the forcing of these components (which is the same in all three cases) we nevertheless see that they differ in their time evolution and again note the disparity between case 1811 and the other two cases. The variation in the solutions must be a consequence of the nonlinearity of the problem and of the interaction of the zonal field with the waves since there can be no self-interaction in the zonal flow. This fact is most notable in the decrease

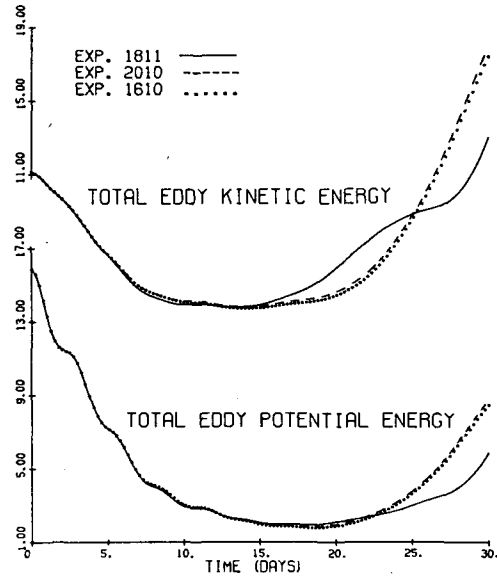

FIG. 7. Time development of total eddy potential and kinetic energy (m^2 sec^{-2}) for all three experiments.

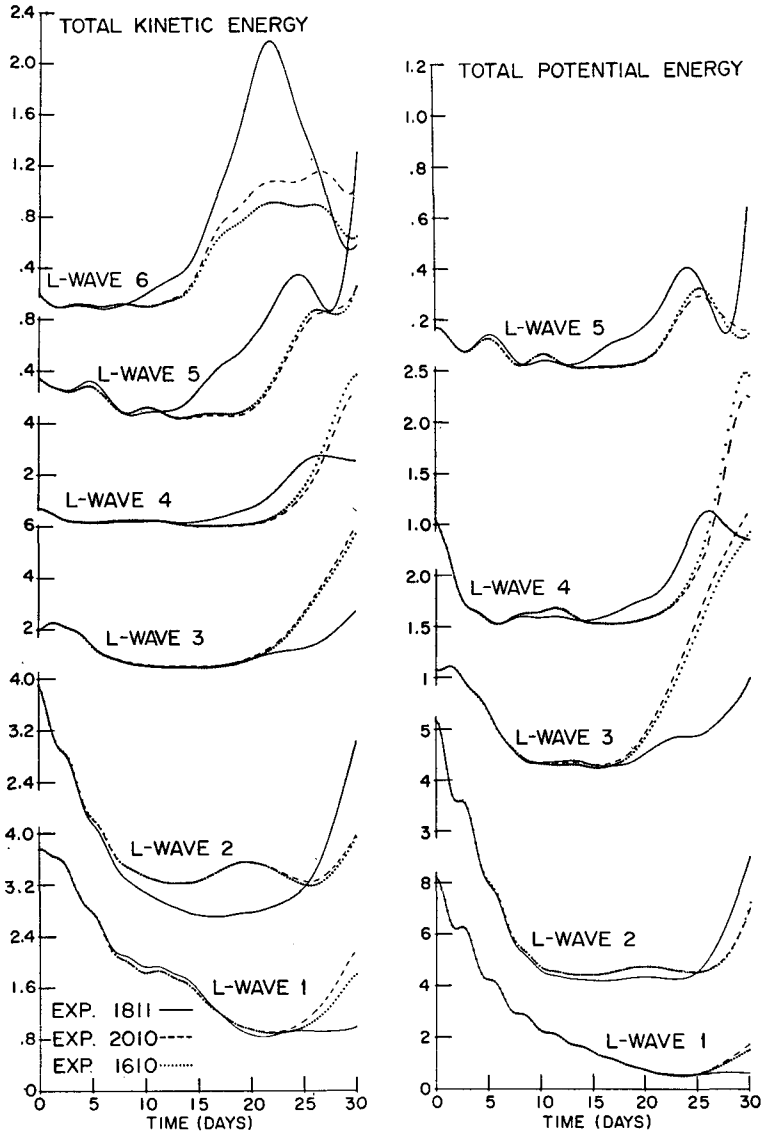

FIG. 8. Time developments of the kinetic and potential energy ($m^2\ sec^{-2}$) in the long planetary waves for all experiments.

with time of the amplitude of components $\gamma=5$. Since the forcing would tend to cause an increase in that component, only nonlinear exchange with the waves can explain the decrease. We shall see how the wave components respond to the zonal field in the following section.

6. Wave characteristics

The total wave energy (sometimes referred to as the eddy energy) may be characterized as the energy in the total flow minus that in the zonal field. We describe both the kinetic and potential eddy energy as a function of time for all three experiments in Fig. 7. We note that there is a decrease of energy initially for about 15 days—wave energy going into the zonal field—after which the wave energy increases. During the decrease period, all experiments have similar development, but after this time experiment 1811 deviates from the other two which remain alike. This development is consistent with the zonal flow as seen in Fig. 5.

The time development of the planetary waves is next described in Fig. 8 for the first six waves ($1\leqslant l\leqslant 6$) for both K_l and A_l and all three experiments. Since most of the amplitude in the wave domain is in these components, they effectively account for the variation observed in Fig. 7. Most apparent from the figure is again the deviation of experiment 1811 from the other two, although the time at which significant differences occur varies for each wave. One could reasonably conclude that larger differences begin when the wave

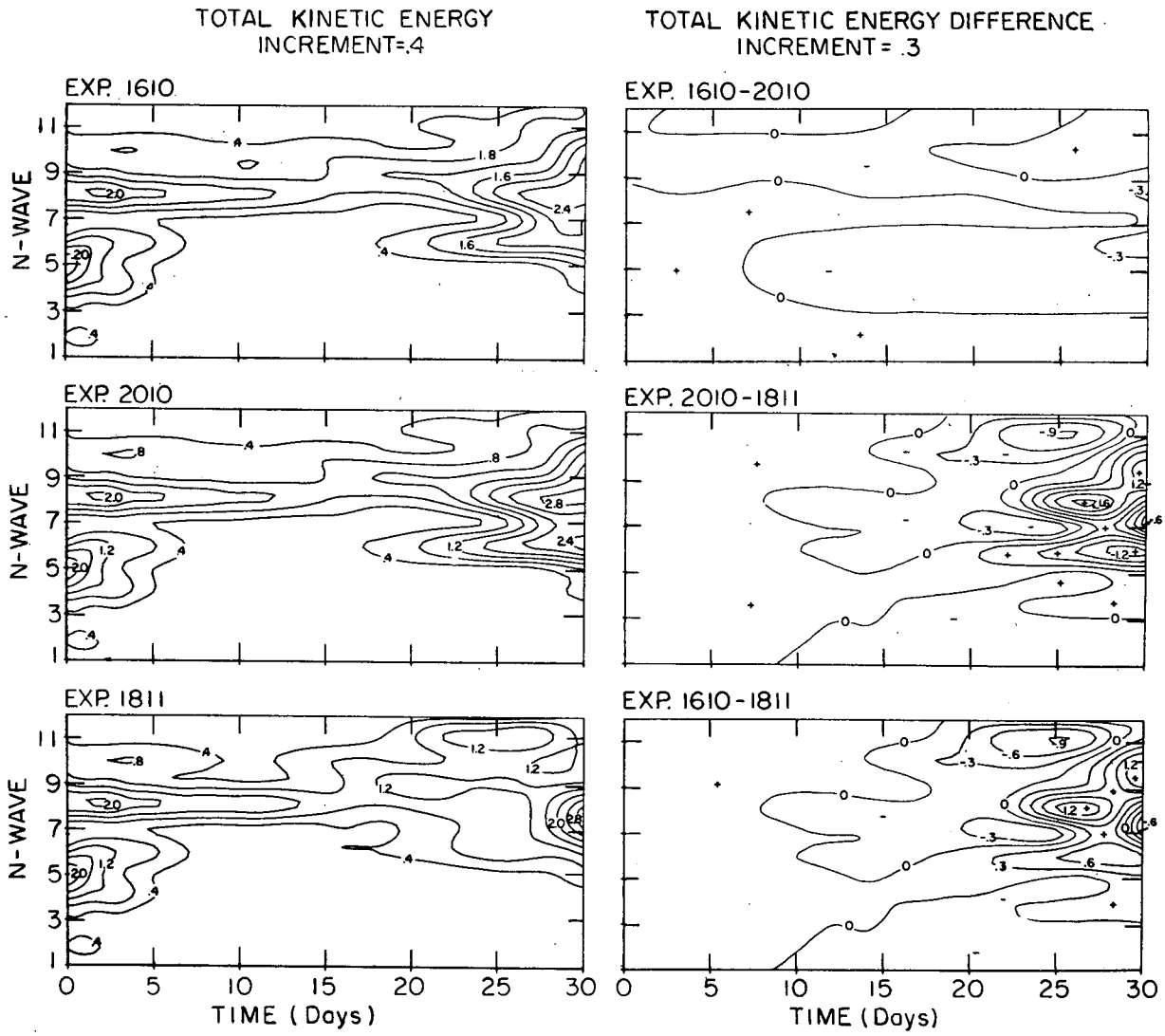

FIG. 9. Time development of kinetic energy and kinetic energy difference (m^2 sec^{-2}) between all combinations of two experiments for the largest two-dimensional scales ($1 \leqslant n \leqslant 12$) with the forcing modes removed.

amplitude starts to grow and nonlinear exchange among the wave components becomes prominent. Thus we see that wave $l=6$ shows deviations among the experiments at the earliest time and also begins to show a variation between experiments 1610 and 2010 before the end of the integration period. Significant differences may also be noted in the available potential energy for waves $l=3$ and 4.

In terms of two-dimensional scale, the amplitude development of the various scales for K_n, $1 \leqslant n \leqslant 12$, is described for all three experiments on a time section with wave amplitude analyzed. These time sections (similar to Fig. 5) may be seen in Fig. 9 together with the difference fields where we analyze the difference in K_n between two experiments. In these analyses the forcing components have been removed ($\gamma=1$, 3, 5) because their amplitude is significantly larger than the other components. Initially it appears that the kinetic energy maximum is in scales 5 and 8, but a shift occurs during time, and the maximum at 30 days depends on the experiment with some consolidation of energy in scales 7–8. The difference field again repeats our previous observations; little difference exists throughout the calculation between experiments 1610 and 2010, but substantial deviations occur between these experiments and 1811. Pronounced variations appear after 20 days of integration, and some oscillation between scales with the largest deviation takes place from 25–30 days.

The similarity of wave development in time between experiments 1610 and 2010 and their difference from 1811 is not confined to only the planetary or largest two-dimensional scales. In Fig. 10 we have plotted the distribution of kinetic energy for all scales resolved

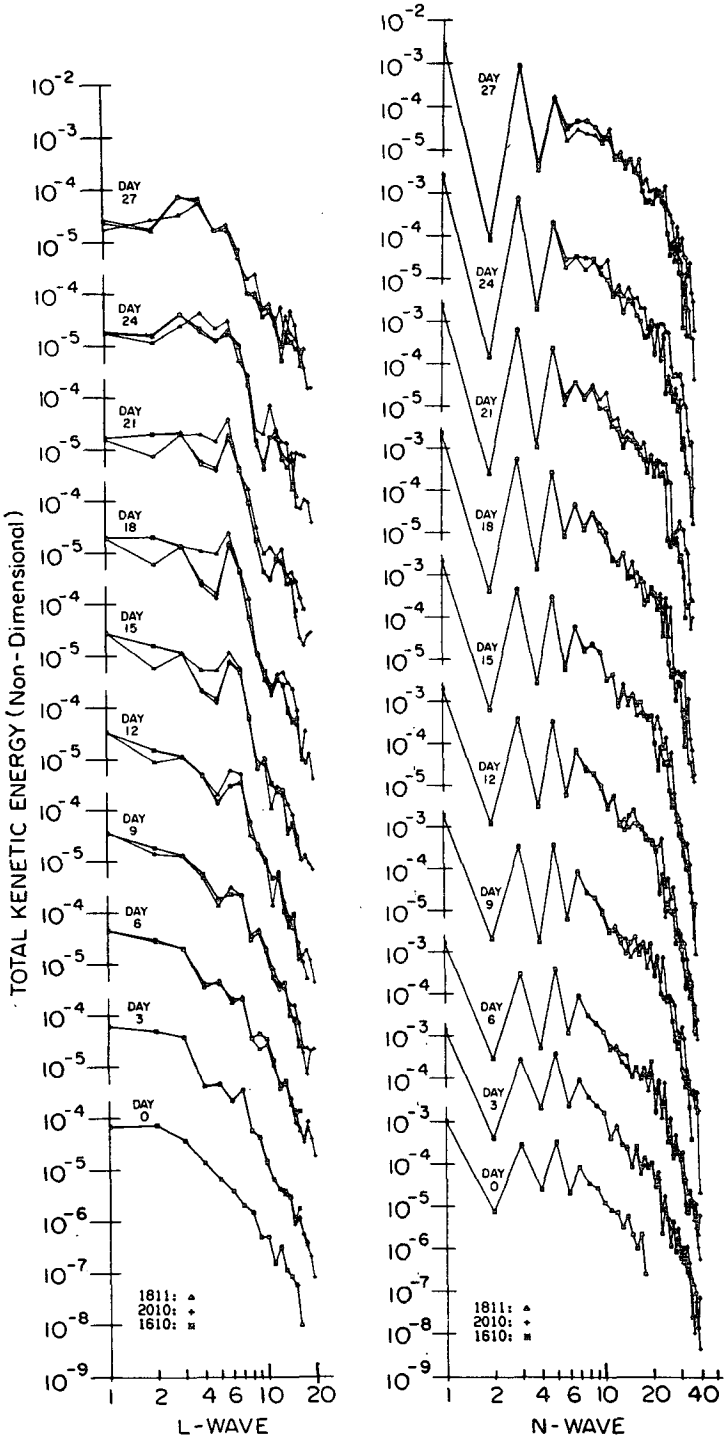

FIG. 10. Spectrum of energy (nondimensional units) as a function of wavenumber for both the planetary wave (l) and the two-dimensional wave (n) for select times during the integration for all experiments.

in the model ($1 \leqslant l \leqslant l_{\max}$ and $1 \leqslant n \leqslant n_{\max}$) for select times during the integration. Despite the almost random behavior of the shorter scales, they do have an expected decay with increasing wavenumber. They also indicate close similarity between experiments 1610 and 2010 and significant differences between these experiments and 1811, differences which begin quite early in the calculation and are noticable already at day 6 into

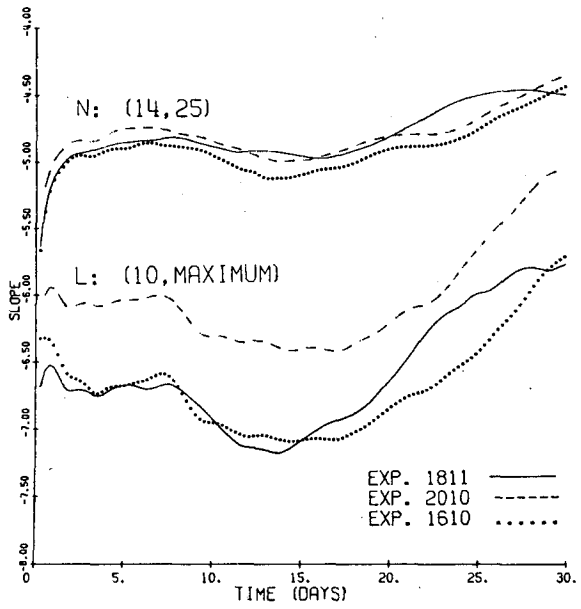

FIG. 11. Time development of slope calculated from the energy in the scale range $10 \leqslant l \leqslant l_{\max}$ and $14 \leqslant n \leqslant 25$ on the assumption of a power law relationship between energy and wave (scale) number.

the integration. The large oscillations in K_n for the larger scales is caused by the forcing zonal components which are included in Fig. 10. We may conclude from this figure that the similarity of calculation between 1610 and 2010 is not confined to the primary energy containing scales, but persists for all scales which are common to both calculations.

The behavior of the shorter scales may be described statistically by fitting the energy to some power of the scale. We have done this by using both the l and n scales. The scale range fit for planetary wavenumbers is $10 \leqslant l \leqslant l_{\max}$ whereas we have chosen $14 \leqslant n \leqslant 25$, a range which has been used to estimate the power in observed data (see Baer, 1972). We describe the time evolution of this statistical power (denoted as slope on a log-log diagram) for all three experiments and for both the n and l scales in Fig. 11. The relative development of the different experiments again shows a similar trend between 1610 and 2010, and both differing substantially from 1811, the difference appearing early in the integration. There is, however, a substantial amplitude difference in the slopes for 1610 and 2010, especially with reference to the planetary wavenumber. This disparity is easily explained by the truncation when one considers Eqs. (7) and (8), since there are more components in the sum for case 2010 than for 1610. In terms of the n-representation, the number of additional elements increases proportionally as the index value increases, whereas in terms of the l-wave, the increase in truncation requires the energy available to spread over a wider wave domain. The values of the slopes are indeed large when one considers that theory might expect a -3. Because of the choice of climatological data, however, one might anticipate larger initial slopes. Whether the solutions would ultimately tend toward the expected -3 over a suitably long integration period would depend entirely on the model characteristics and has not been established for the model under consideration. It is thus sufficient to note the close correspondence between 1610 and 2010 as contrasted to 1811.

7. Conclusions

Previous calculations by the writers (Baer and Alyea, 1971) with a two-level, quasi-geostrophic, thermally forced model indicated that when integrating the spectral domain, predictability as a function of time was strongly dependent on truncation. Nevertheless, for the model in question, when 10 degrees of freedom in latitude were used, the integrations with 14 and 16 planetary waves were remarkably similar over a period of 30 days. By contrast, the integration with 16 planetary waves and 8 degrees of latitudinal freedom showed marked deviations from the two experiments which compared so favorably. In all cases, the only change in the different integrations was in the truncation; i.e., the initial conditions, the model, the boundary conditions, and the forcing were all unchanged.

To isolate the relative effects of latitudinal and longitudinal truncation on predictability, three further experiments were performed with the same model but with slightly different forcing and initial conditions from the previous experiments. These new calculations were for truncations with 16 and 20 planetary waves and 10 degrees of latitudinal freedom (denoted as the 1610 and 2010 experiments) and for 18 planetary waves and 11 degrees of latitudinal freedom (1811 experiment). The calculations were performed for 30 days and the results of various parameters from each experiment were compared as they developed in time.

The results indicate that given 10 degrees of freedom in latitude, comparable results may be achieved for the model under question with a truncation of either 16 or 20 planetary waves over a 30-day integration period. By inference with the previous study, one might extend this statement to include a truncation of 14 planetary waves. This correspondence is seen not only in the gross properties of the flow such as the total energy or the eddy energy, but in the zonal flow and its components, as well as in the individual eddy components. The issue is substantially complicated by the results of the 1811 experiment, however, which showed significant deviation from the other two experiments, especially after 15 days. This 15-day figure should not be interpreted in any absolute sense since there is strong indication that a lack of wave instability in the initial state caused a retardation in wave development. Thus, we may conclude that 10 degrees of latitudinal resolution is insufficient to yield "adequate" solutions over the integration period and that perhaps the model

is substantially more sensitive to latitudinal rather than longitudinal resolution.

The issue is certainly not conclusively resolved. Truncation of the spectral model was made in a "rhomboidal" sense, a procedure in general favor but more recently subject to question (see Baer, 1972). If a "triangular" truncation were applied, only one scale index would be involved in the truncation experiment thus simplifying the comparisons and perhaps isolating the important scales related to predictability. We therefore recommend further experiments of the sort described herein but with triangular truncation and perhaps somewhat more model sophistication. In conclusion, it is essential to note that the processes studied here involve the ability of a model to reproduce similar results under various truncations and *not* the model's ability to reproduce "reality," although the model has been chosen because of its representativeness of the earth's atmosphere.

Acknowledgments. Programming assistance has been provided by Carl Wade and James J. Sterken. This research has been supported by the Atmospheric Sciences Section of the National Science Foundation through Grant GA-36409 to the University of Michigan. The National Center for Atmospheric Research, sponsored by the National Science Foundation, provided computer time for this research.

REFERENCES

Baer, F., 1972: An alternate scale representation of atmospheric energy spectra. *J. Atmos. Sci.*, **29**, 649–664.

——, and F. N. Alyea, 1971: Effects of spectral truncation on general circulation and long range prediction. *J. Atmos. Sci.*, **28**, 457–480.

——, and T. J. Simons, 1970: Computational stability and time truncation of coupled nonlinear equations with exact solutions. *Mon. Wea. Rev.*, **98**, 665–679.

Charney, J. G., 1971: Geostrophic turbulence. *J. Atmos. Sci.*, **28**, 1087–1095.

Crutcher, H. L., and J. M. Meserve, 1970: Selected level heights temperatures and dew points for the northern hemisphere. NAVAIR-50-1C-52, Naval Weather Service Command.

Davis, P. A., 1963: An analysis of the atmospheric heat budget. *J. Atmos. Sci.*, **20**, 5–22.

Ellsaesser, H. W., 1966: Evaluation of spectral versus grid methods of hemispheric numerical weather prediction. *J. Appl. Meteor.*, **5**, 246–262.

Grammeltvedt, A., 1969: A survey of finite-difference schemes for the primitive equations for a barotropic fluid. *Mon. Wea. Rev.*, **97**, 384–404.

Kraichnan, R. H., 1967: Inertial ranges in two-dimensional turbulence. *Phys. Fluids*, **10**, 1417–1423.

Lettau, H. H., 1954: A study of the mass momentum and energy budget of the atmosphere. *Arch. Meteor. Geophys. Bioklim.*, **A7**, 133–157.

Lorenz, E. N., 1960: Energy and numerical weather prediction. *Tellus*, **12**, 364–373.

——, 1967: *The Nature and Theory of the General Circulation of the Atmosphere.* Geneva, World Meteorological Organization, 161 pp.

——, 1969: The predictability of a flow which possesses many scales of motion. *Tellus*, **21**, 289–307.

Machenhauer, B., and E. Rasmussen, 1972: On the integration of the spectral hydrodynamical equations by a transform method. Rept. No. 3, Inst. Teoret. Meteor., Copenhagen, 44 pp.

Mintz, Y., 1958: Design of some numerical general circulation experiments. *Bull. Res. Council Israel*, **7G**, 67–114.

Miyakoda, K., R. F. Strickler, C. J. Nappo, P. L. Baker and G. D. Hembree, 1971: The effect of horizontal grid resolution in an atmosphereic circulation model. *J. Atmos. Sci.*, **28**, 481–499.

Phillips, N. A., 1956: The general circulation of the atmosphere: A numerical experiment. *Quart. J. Roy. Meteor. Soc.*, **82**, 123–164.

Platzman, G. W., 1960: The spectral form of the vorticity equation. *J. Meteor.*, **17**, 635–644.

Sellers, W. D., 1965: *Physical Climatology.* The University of Chicago Press, 272 pp.

Smagorinsky, J., S. Manake and J. L. Holloway, Jr., 1965: Numerical results from a nine-level general circulation model. *Mon. Wea. Rev.*, **93**, 727–768.

Wellck, R. E., A. Kasahara, W. M. Washington and G. De Santo, 1971: Effect of horizontal resolution in a finite-difference model of the general circulation. *Mon. Wea. Rev.*, **99**, 673–683.